

# Preparation of Liposomes Coated Superparamagnetic Iron Oxide Nanoparticles for Targeting and Imaging Brain Glioma

Weijia Chen<sup>1,2</sup>, Yingtian Xu<sup>1,2</sup>, Dicheng Yang<sup>1</sup>, Ping Wang<sup>1</sup>, Yan Xu<sup>1</sup>✉, Jun Zhu<sup>1</sup>, Daxiang Cui<sup>3</sup>

<sup>1</sup>National Engineering Research Center for Nanotechnology, Shanghai, China.

<sup>2</sup>School of Material Sciences and Engineering, Shanghai Jiao Tong University, Shanghai, China.

<sup>3</sup>Institute of Nano Biomedicine and Engineering, Shanghai Engineering Research Centre for Intelligent Diagnosis and Treatment Instrument, Department of Instrument Science and Engineering, School of Electronic Information and Electrical Engineering, Shanghai Jiao Tong University, Shanghai, China.

✉ Corresponding author. E-mail: yxusinap@163.com Tel.: +86-021-34291286

**Received:** Oct. 9, 2021; **Accepted:** May 8, 2022; **Published:** May 10, 2022

**Citation:** Weijia Chen, Yingtian Xu, Dicheng Yang, Ping Wang, Yan Xu, Jun Zhu, and Daxiang Cui, Preparation of Liposomes Coated Superparamagnetic Iron Oxide Nanoparticles for Targeting and Imaging Brain Glioma. *Nano Biomed. Eng.*, 2022, 14(1): 71-80.

**DOI:** 10.5101/nbe.v14i1.p71-80.

## Abstract

Effective and specific diagnostic imaging of brain glioma remains a challenge. Magnetic nanoparticles are actively being developed as contrast agents for diagnosis of tumor. In this work, we developed the targeted magnetic nanoparticles as T<sub>1</sub>-positive magnetic resonance imaging (MRI) contrast agents. Zn-doped Fe<sub>3</sub>O<sub>4</sub> NPs were synthesized by solvothermal method, coated with liposome and conjugated to a tumor-penetrating peptide (RGERPPR). The effect of zinc doping on the magnetic properties of Fe<sub>3</sub>O<sub>4</sub> nanoparticles was studied. Zn<sub>0.4</sub>Fe<sub>2.6</sub>O<sub>4</sub>-PEG nanoparticles exhibited T<sub>1</sub> MR contrast enhancement. Cytotoxicity assay indicated that nanoparticles have good biocompatibility and low toxicity. And the in vitro cellular uptake assays on U87 cells confirmed that the conjugation of RGERPPR increased the uptake of the Zn<sub>0.4</sub>Fe<sub>2.6</sub>O<sub>4</sub> NPs. In vivo MR imaging showed the contrast enhance of U87 brain glioma in rat model after injection.

**Keywords:** Iron oxide nanoparticles, Magnetic resonance imaging, Tumor penetrating peptide, Brain glioma imaging

## Introduction

Gliomas is one of the most common intracranial malignant tumors which usually occurs in the neuroectoderm and originated from the supportive cells of brain, comprising about 30 percent of primary brain tumors and central nervous system tumors. Glioblastoma is the most aggressive and common type of malignant brain tumor [1]. Strong invasive ability, poor prognosis and easy recurrence are its main clinical features which threaten the survival of the patient [2].

Early diagnosis [3, 4] of this malignant disease is an effective way to improve the prognosis of the disease. As a non-invasive, non-ionizing, non-radiative medical imaging technique, magnetic resonance imaging (MRI) plays an indispensable role in the diagnosis and directs towards the correct treatment [5].

MRI output the NMR signal based on the different T<sub>1</sub> and T<sub>2</sub> relaxation of proton in tissues and the signal is processed to form an image of the body. While MRI has high spatial resolution and excellent soft tissue contrast, it also suffers disadvantages of low

sensitivity as well as nonspecific targeting. To enhance contrast by either suppressing or highlighting certain tissue structures, some paramagnetic materials are applied as contrast agents, like gadolinium (Gd), and manganese (Mn) in the stable chelate form. However, these contrast agents are deficient in short imaging time, fast diffusion and even causing side effects to patients. Therefore, developing novel MRI agents are needed to increase the imaging effect by improving either  $T_1$  or  $T_2$ -weighted relaxation. Typically,  $T_1$  agents shorten  $T_1$  and enhance the  $T_1$  signal by directly acting on the hydrogen nucleus and paramagnetic metal ions in the water,  $T_2$  agents shorten the  $T_2$  relaxation time and reduce the  $T_2$  signals by interfering the external magnetic environment [4]. Superparamagnetic iron oxide nanoparticles (SPION) are extensively explored as  $T_2$  contrast agent due to their excellent biocompatibility, easy biodegradability, potential nontoxicity and distinct magnetic properties [6-8]. Since iron ion contains five unpaired electrons, the iron oxide nanoparticles can also be used as a  $T_1$  contrast agent and magnetic properties are closely related to their size [9-12]. With the decrease of size,  $T_1$  effect are strengthened and  $T_2$  effect are suppressed [13]. Furthermore, limited literatures have reported on  $T_1$ -weighted MRI of brain glioma with high specificity.

Meanwhile, for *in vivo* applications, surface modification of iron oxide nanoparticles is introduced to increase the dispersity and blood circulation [14, 15]. Different materials are applied to encapsulate MNPs, including organic molecules [16], polymers [17-20] and inorganic materials [21, 22]. Moreover, with an appropriate coating, the reactivity of nanoparticles is also increased and molecular targets are able to link to the nanoparticles through the surface-modified functional groups to improve specific targeting of NPs [23-26].

Especially, peptides with high affinity to tumor-associated markers have been used to synthesis multifunctional nanoparticles for targeted cancer imaging to improve biodistribution and efficiency of contrast agents [27, 28]. For example, RGERPPR is a type of C-end R peptides, which has a high binding affinity to NRP-1 and triggers cellular internalization and tissue penetration. Meanwhile, Neuropilin-1 (NRP-1), known as a mediator of vascular permeability induced by VEGF, is overexpressed in many tumor cells including glioma [29, 30]. NRP-1 is one of essential participants in tumor angiogenesis, metastasis and regulation of vascular permeability and an ideal

target spot for fabrication of enhanced medical imaging NPs [31].

In this study, we prepared RGERPPR-functionalized and liposome coated iron oxide nanoparticles to enhance the magnetic resonance imagination with comparable specificity towards brain glioma. Firstly, we synthesized oleic modified iron oxide nanoparticles and investigated their magnetic performance. Secondly, we conjugated RGERPPR to the surface of liposomes and coated iron oxide nanoparticles with the liposome. Then we tested their targetability to U87 glioblastoma cells *in vitro* and MRI performance *in vivo*. The results have indicated the as prepared SPION has excellent target ability and the corresponding satisfactory MRI performance towards glioma tissues.

## Experimental

### Synthesis and characterization of the MNPs-DSPE-PEG-RGERPPR

#### Preparation of Zn-doped $Fe_3O_4$ nanoparticles

The oleic acid-coated Zn-doped  $Fe_3O_4$  nanoparticles were prepared through hydrothermal method. Firstly, 0.683 g of  $FeSO_4 \cdot (NH_4)_2 \cdot 6H_2O$  and 0.27 g of  $ZnSO_4 \cdot 7H_2O$  were dissolved in 20 mL of deionized water, followed by an ultrasonic bath. Secondly, 10 mL of oleic acid, 10 mL of ethanol and 1 g of NaOH were mixed and magnetic stirred until forming a uniform white emulsion. Then, above two solutions were mixed together and stirred for another 30 min to form a dark brown liquid, the mixture was transferred to the 50 mL Teflon-lined autoclave and reacted at 230 °C for 15 hours. After magnetic separation and washing by ethanol for at least 5 times, the Zn-doped  $Fe_3O_4$  nanoparticles (MNPs) were finally obtained and kept in cyclohexane.

#### Synthesis of peptide-DSPE conjugate

The peptide (CRGERPPR) was purchased from GL Biochem (Shanghai) Ltd. And used as received without any modification. The linkage of peptide with maleimide-modified DSPE was achieved through coupling of maleimide groups on DSPE-PEG2000-Mal with thiol group on peptides. Briefly, 2.15 mg of peptide (CRGERPPR) was dispersed in 1 mL PBS, and 0.5 mL of DFM containing 8.9 mg DSPE-PEG2000-MAL was added. Then, 10  $\mu$ L of 60 mM Tris (2-carboxyethyl) phosphine (TCEP) hydrochloride was added into the mixture to stabilize thiol groups. After thoroughly mixed, the solution was ultrasonicated to remove the bubbles in the liquid. Furthermore, the

mixture was magnetic stirred at room temperature for 2 hr, and purified by dialysis. The final product of peptide-DSPE was freeze-dried [32, 33], and stored at 4 °C for further use.

### Synthesis of $Zn_{0.4}Fe_{2.6}O_4$ -PEG-RGERPPRs

17 mg of peptide-DSPE, was dissolved in 5 mL chloroform and 5 mg NMPs was dispersed in 5 mL hexane, respectively. The above two solutions were mixed together by ultrasonic and then transferred into a round flask. Afterwards, 5 mL of deionized water was added into the mixture drop by drop to form a micro-emulsion under constant magnetic stirred for 1 hr, followed by rotary evaporation under 70 °C for 15 minutes to remove organic solvents. The final product of  $Zn_{0.4}Fe_{2.6}O_4$ -PEG-RGERPPR was purified through magnetic separation for 3 times, then, was collected and dispersed in deionized water at 4 °C for storage.

### Characterizations

Transmission electron microscopy (TEM) images were taken with a JEOL 2011 microscope (Japan) operated at 200 kV. MNPs coated with liposomes are negatively stained with 4% phosphotungstic acid and collected using carbon-film-covered copper grids for analysis. Wide-angle XRD patterns were recorded on a  $\theta/\theta$ /max-2600PC diffractometer using Cu radiation (45 kV, 20 mA, 10° from 5 to 90°). Fourier-transform infrared (FT-IR) spectra were tested through Nicolet Fourier spectrophotometer (F-1000, Hitachi, Japan). The DLS measurements were conducted on a Nano-ZS Zetasizer (Malvern Instruments, Westborough, MA). The magnetic properties of the products were characterized by Magnetic Property Measurement System (MPMS) in an applied magnetic field sweeping from -20 to 20 kOe.

MR performance of the MNPs were conducted on a 0.5 T MR scanner (Shanghai NIUMAG corporation, Shanghai, China). The measurement parameters were set as follows: repetition times (TR) = 900 ms, multiple echo time (TE) = 18.2 ms,  $\alpha = 90^\circ$ , base resolution =  $256 \times 256$ , FOV =  $10 \times 10$  cm, and slice thickness = 1 mm. Relaxation rate  $R(R=1/T)$  were calculated with T of Fe concentration. The  $T_1$  and  $T_2$  relaxivity was calculated by linear fitting the inverse  $T_1$  and  $T_2$  relaxation time ( $1/T_1$  or  $1/T_2$ ) as a function of Fe concentration.

### Assessment of NH13-PEG-DSPE-MNPs interactions with U87 glioma cells

#### U87 glioma cells

The U87 glioma cells were cultured in DMEM

medium, supplemented with 10% fetal bovine serum, 100 units/mL of penicillin G, and 100  $\mu$ g/mL of streptomycin. In all experiments, cells were maintained in culture dishes (Nunc; Thermo Fisher Scientific, Waltham, MA, USA) at 37 °C in a humidified 5%  $CO_2$ /95% air atmosphere.

### Cell viability

CCK-8 assay was used to evaluate the cytotoxicity of nanoparticles. The CCK-8 reagent can be reduced by the dehydrogenase in the mitochondria of the cell. U87 cells were seeded in 96-well plates at the density of 2000 cells/well, and cultured in a 5%  $CO_2$  incubator at 37 °C for 24 hours. After re-stabilization of the cell state,  $Zn_{0.4}Fe_{2.6}O_4$ -PEG-RGERPPR with various concentrations (100~500  $\mu$ g/mL) were added into each well and cultured for 24 hr. Then, each well was washed with PBS and added into 0.1 mL of DMEM containing 10% CCK solution, and continue incubated for 2-4 hours. The absorbance of each well was measured at 450 nm via a microplate reader (BIO-RAD680, USA). According to the formula: cell viability (%) = (average absorbance of the treatment group/average absorbance of the control group  $\times$  100%), the value of cytotoxicity was calculated.

### Tumor cellular uptake of NPs *in vitro*

The U87 cells were seeded in a 6-well microplate at the density of  $5 \times 10^4$  cells/well. After incubation for 24 h, the cells were treated with 50  $\mu$ g/mL  $Zn_{0.4}Fe_{2.6}O_4$ -PEG/FITC or  $Zn_{0.4}Fe_{2.6}O_4$ -PEG-RGERPPR/FITC NPs for 8 h at 37 °C. Then, the cells were washed thrice with PBS, fixed with 4% paraformaldehyde solution, sequential stained with DAPI and observed using a confocal laser scanning microscope (Leica, DMI4000 B, Germany).

### *In-vivo* study

#### Building of tumor animal model

All manipulations were performed in accordance with procedures approved by the ethics committee (Shanghai Jiao Tong University). All animal procedures were conducted under a protocol approved by the IACUCs. 5-week-old nude mice (~25 g, Shanghai SLAC Laboratory Animal Center, Shanghai, China) were injected with 5 U87MG cells in the right forelimb. When the tumors reached an approximate size of 100  $mm^3$  in volume, the tumor-bearing mice were randomly divided into 2 groups as follows: control group and treated group (each group had 3 mice). The mice were administered saline and solution of  $Zn_{0.4}Fe_{2.6}O_4$ -

PEG-RGERPPR (100 $\mu$ L, 10 mg/kg) through tail vein injection, then followed by  $T_1$ -weighted MRI.

### MRI experiments

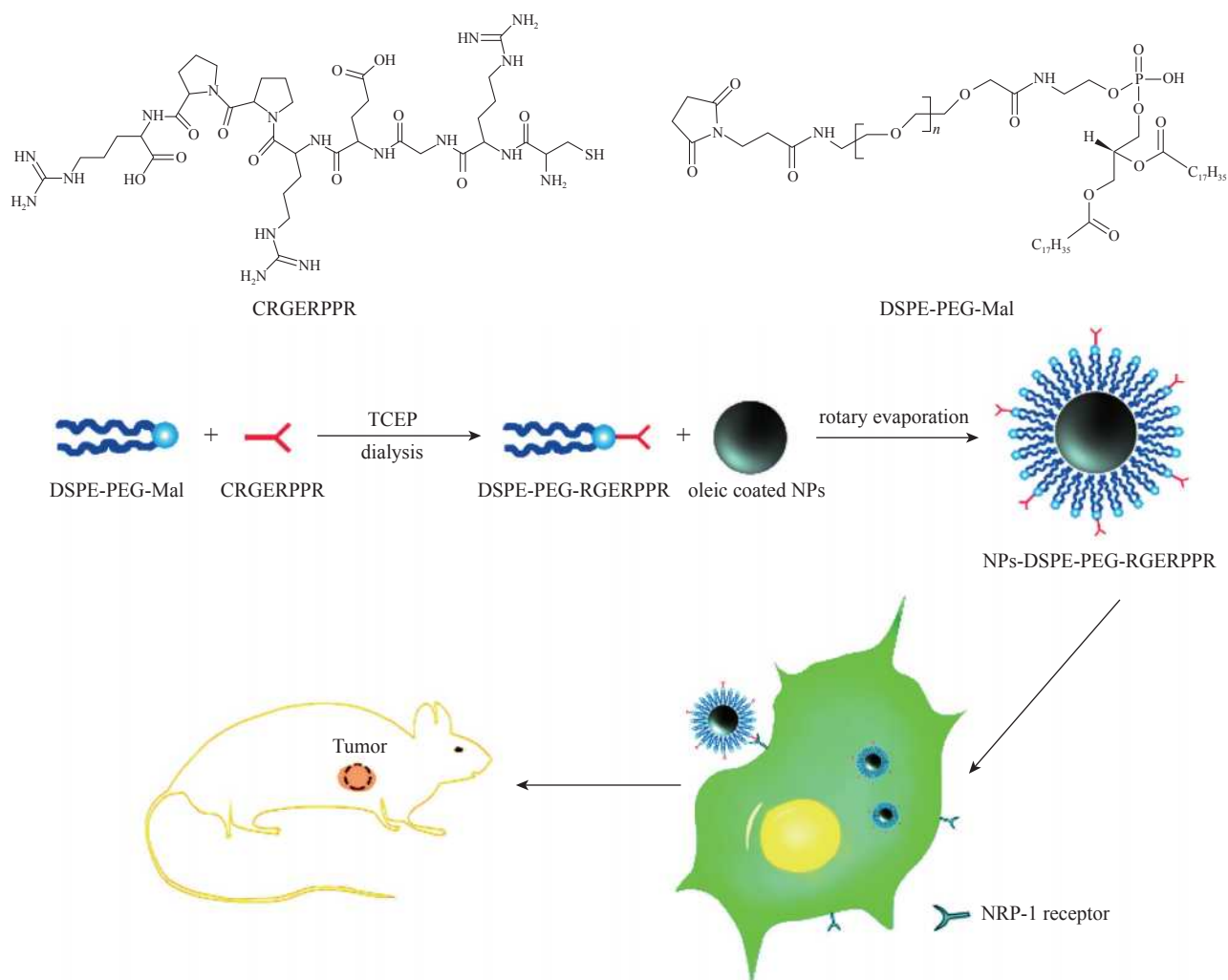
MRI studies were conducted in a 0.5 T Magnetic Resonance Imaging Analyzer (MesoMR23-060H-I). The sequence used was a Rapid Acquisition with Relaxation Enhancement (RARE). High-resolution images were obtained 2 hr after injection of the solution using a  $T_1$ -weighted RARE sequence with the following parameters: TR = 400 ms, TE = 18.2 ms, TR/TE = 22, matrix = 256  $\times$  256,  $\alpha$  = 0 $^\circ$  and 90 $^\circ$ , FOV = 10  $\times$  10 cm, and slice thickness = 2.5 mm. After acquiring the images, the magnitudes of image intensities  $T_1$  were measured with manually bright regions of interest for samples.

## Results and Discussion

The principle of the prepared imaging agents is

depicted in Scheme 1. Briefly, the strategy to prepare  $Zn_{0.4}Fe_{2.6}O_4$ -PEG-RGERPPR NPs involve three steps, consisting of synthesis of  $Zn_{0.4}Fe_{2.6}O_4$  nanoparticles by solvothermal method, conjugation of peptide to DEPS-PEG-Mal and surface coating by reverse rotary evaporation. REGRPPR peptide, as the special ligand of NRP-1 receptor, is able to compensate for the EPR effect and penetrate through the tumor. Then, modified nanoparticles could be targeted internalized by U87 tumor cells and perform MRI in mice.

We first studied the magnetic properties of  $Fe_3O_4$  NPs and the effect of Zinc doping to determine the efficacy of serving as MRI contrast agent (Fig. 1). At 300 K, the nanoparticles with different Zinc doping amount display magnetization curves with low remanence and coercivity, which demonstrated superparamagnetic behavior. The saturation magnetization ( $M_s$ ) of  $Fe_{3-x}Zn_xO_4$  nanoparticles with zinc amount of 0.2, 0.4, 0.6, 0.8 and 1.0 were respectively 44.8, 60.0, 59.5, 39.5 and 32.3 emu/g



**Scheme 1** Synthesis and function of  $Zn_{0.4}Fe_{2.6}O_4$ -PEG-RGERPPR magnetic NPs in vitro and *in vivo*.

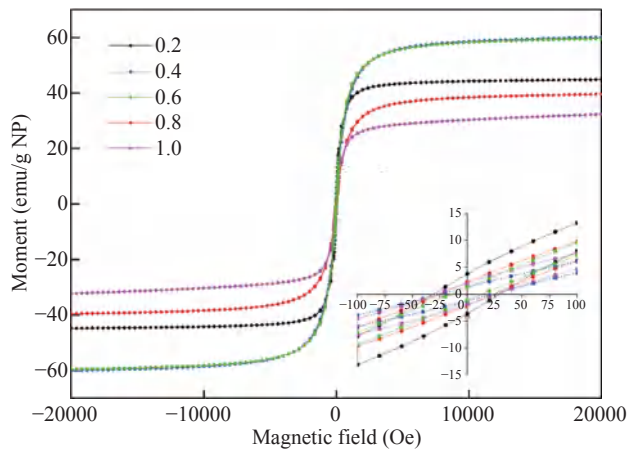


**Fig. 1** Normalized magnetization curves of  $\text{Fe}_{3-x}\text{Zn}_x\text{O}_4$ , the values of  $x$  were 0.2, 0.4, 0.6, 0.8, 1.0.

nanoparticle. With the improvement of Zinc amount, the saturation magnetization rised and then decreased.

In inverse spinel crystal structure of  $\text{Fe}_3\text{O}_4$ ,  $\text{Fe}^{3+}$  and  $\text{Fe}^{2+}$  occupy the tetrahedral and octahedral sites. The magnetic spins of the ions are parallel to each other, but the spin directions of ions at the octahedral site and the tetrahedron are opposite. Therefore, some of the magnetic moments is offset, and the system exhibits only a part of  $\text{Fe}^{2+}$  magnetism in the octahedral site.  $\text{Zn}^{2+}$  has a higher tetrahedron priority and thus reduces the offset magnetic moment. However, zinc is a non-magnetic ion and reduces superexchange effects. When the amount of zinc ions reaches a certain value, the two effects reach equilibrium, at the saturation magnetism is the largest. Therefore, zinc amount of 0.4 was chosen with sequential modification with targeting ligand for MRI of nerve tumor.

The crystal structure of MNPs was characterized by XRD (Fig. 2). The diffraction pattern has seven strong peaks at  $29.8^\circ$ ,  $35.1^\circ$ ,  $42.7^\circ$ ,  $53.0^\circ$ ,  $56.6^\circ$ ,  $62.2^\circ$ ,  $73.7^\circ$ , corresponding to (220), (311), (400), (422), (511), (440), and (533) of the magnetic ( $\text{Zn}_{0.4}\text{Fe}_{2.6}\text{O}_4$ ) reference (JCPDS card No. 19-0629), respectively. Inverse spinel crystal structure and highly crystalline nature were indicated from the sharp and intense diffraction peaks.

The morphology and size of the  $\text{Zn}_{0.4}\text{Fe}_{2.6}\text{O}_4$  and  $\text{Zn}_{0.4}\text{Fe}_{2.6}\text{O}_4$ -DSPE-PEG NPs were characterized by TEM (Fig. 3). Both particles showed a spherical shape and a highly uniform particle size distribution. Furthermore, after liposome coating, clear core-shell nanostructure of  $\text{Zn}_{0.4}\text{Fe}_{2.6}\text{O}_4$ -DSPE-PEG-CRGERPPR NPs have been observed when negative staining with tungsten phosphate. The average particle sizes calculated from the statistical analysis of the oleic

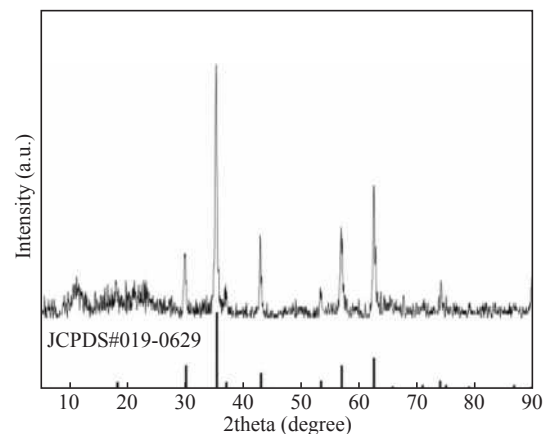


**Fig. 2** X-ray diffraction patterns of  $\text{Zn}_{0.4}\text{Fe}_{2.6}\text{O}_4$  NPs.

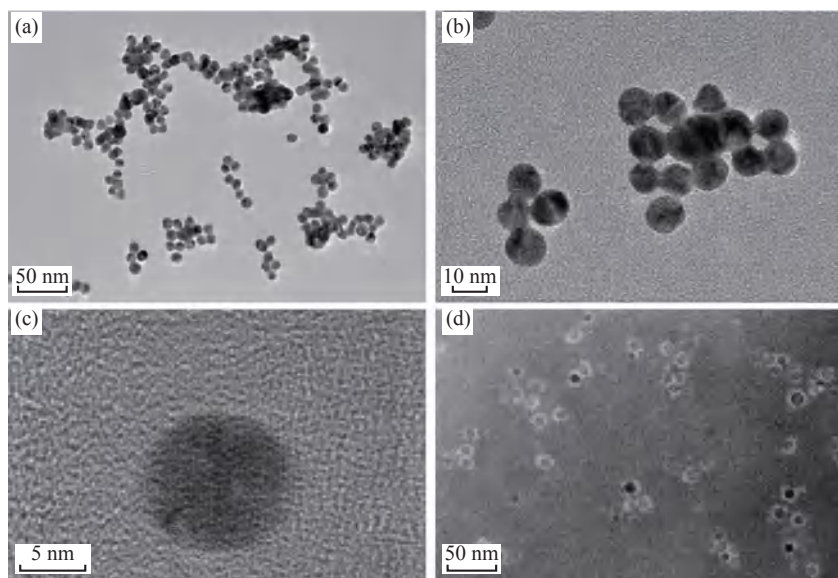


**Fig. 3** Typical TEM images of (a)-(c)  $\text{Zn}_{0.4}\text{Fe}_{2.6}\text{O}_4$  NPs (d) and  $\text{Zn}_{0.4}\text{Fe}_{2.6}\text{O}_4$ -DSPE-PEG NPs.

coated  $Zn_{0.4}Fe_{2.6}O_4$  and  $Zn_{0.4}Fe_{2.6}O_4$ -DSPE-PEG NPs were 9 nm and 17.2 nm, respectively.

Compared with gadolinium, iron oxide nanoparticles have good enhancement effect and relatively small biological toxicity. But there are still some problems when it is used in MR imaging. After entering into the blood, magnetic nanoparticles will be adsorbed by plasma proteins non-specifically, resulting in rapid phagocytosis and clearance by res system (macrophages). In addition, due to their high specific surface area, magnetic nanoparticles are easily agglomerate in the blood and lead to the reduction of superparamagnetism and MRI capability. Therefore, functional modification of magnetic nanoparticles is need to improve its stability and biocompatibility, making it more suitable for in vivo applications. Surface modification of iron oxide nanoparticles and the application of liposome materials with good biocompatibility can increase the dispersion and prolong blood circulation. With appropriate coating, the molecular target would be connected to nanoparticles through functional groups, and so the specific targeting ability was achieved.

We then carried out FT-IR analysis to confirm the successful linkage of targeting ligand on surface of MNPs. As presented in Fig. 4, after the conjugation of DSPE-PEG-Mal and RGERPPR, the N-H stretch band at  $3200-3600\text{ cm}^{-1}$  and the C=O stretch band at about  $1700\text{ cm}^{-1}$  appeared stronger in the spectrum of DSPE-PEG-RGERPPR, that can be attributed to the increased number of peptide bonds. The absorption peak at  $650-750\text{ cm}^{-1}$  belongs to the stretching vibration mode of Fe-O bonds in  $Zn_{0.4}Fe_{2.6}O_4$ . After coating of liposome, the new band at around  $3000-2800\text{ cm}^{-1}$  should be assigned to the stretching vibrations modes

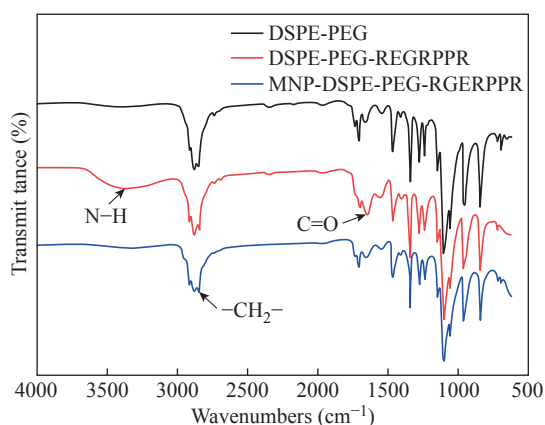


**Fig. 4** FTIR spectrum of DSPE-PEG, DSPE-PEG-RGERPPR and  $Zn_{0.4}Fe_{2.6}O_4$ -DSPE-PEG-RGERPPR NPs.

of  $-CH_2$  groups of PEG. These results suggested that  $Zn_{0.4}Fe_{2.6}O_4$  had been coated with DSPE-PEG-RGERPPR.

Moreover, the successful conjugation of  $Zn_{0.4}Fe_{2.6}O_4$  NPs and DSPE-PEG-RGERPPR was also confirmed by DLS measurement. As shown in Fig. 5, the average hydrodynamic diameters were increased from 52.0 nm of the  $Zn_{0.4}Fe_{2.6}O_4$  NPs to 108.2 nm of the  $Zn_{0.4}Fe_{2.6}O_4$ -PEG and 110.7 nm of the  $Zn_{0.4}Fe_{2.6}O_4$ -PEG-RGERPPR. The hydration radius of nanoparticle is related to whether it can effectively overcome the biological defense system and vascular obstacles. It has been reported that magnetic nanoparticles with relative smaller hydrodynamic size have stronger EPR effect and they are easier to pass through the gap (100 nm to several microns) on tumor vessels.

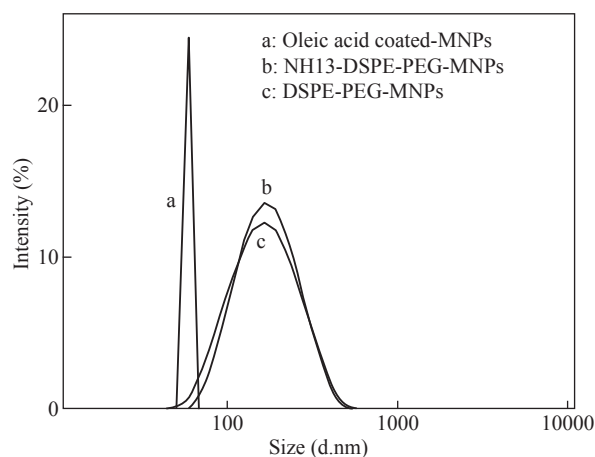


**Fig. 5** Size distribution of  $Zn_{0.4}Fe_{2.6}O_4$ ,  $Zn_{0.4}Fe_{2.6}O_4$ -PEG and  $Zn_{0.4}Fe_{2.6}O_4$ -PEG-RGERPPR NPs.

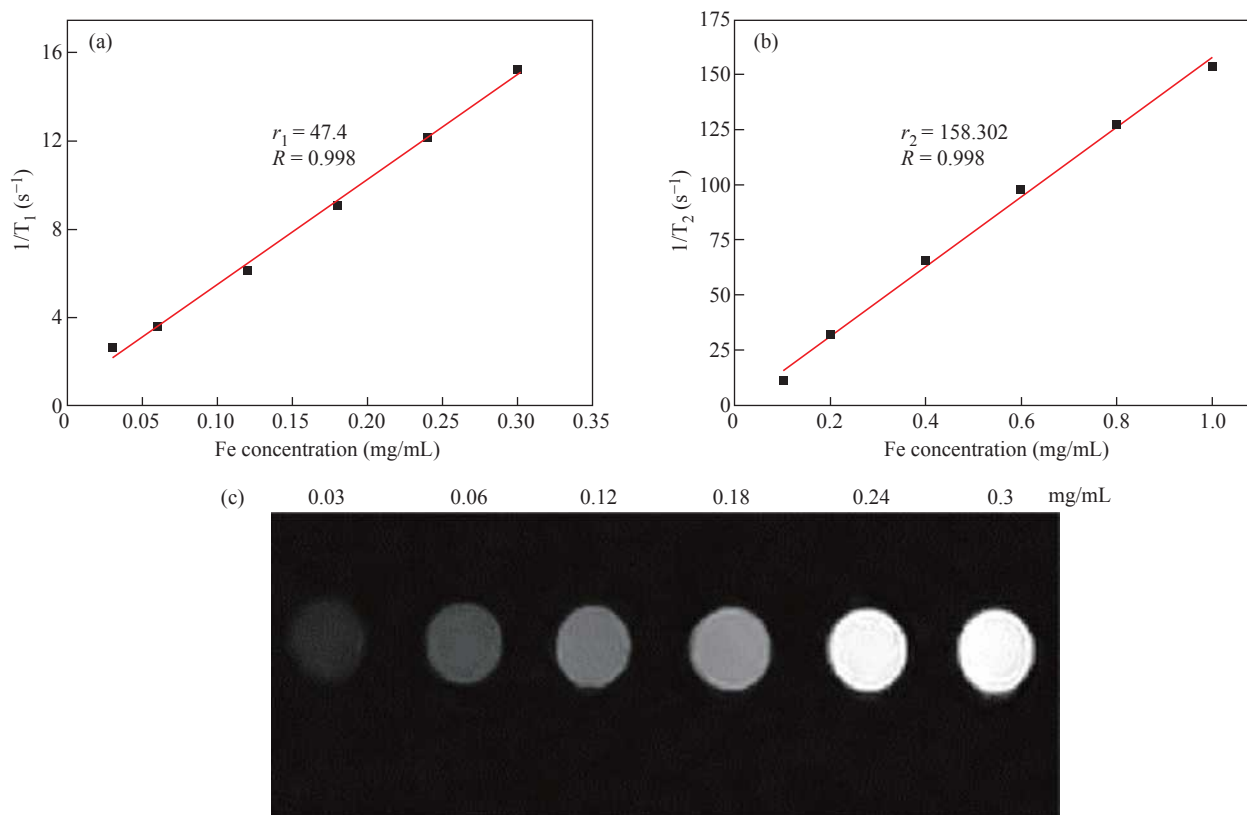
In Table 1,  $Zn_{0.4}Fe_{2.6}O_4$ -PEG-RGERPPR showed more positive charges (4.7 mV) than that of  $Zn_{0.4}Fe_{2.6}O_4$  NPs (-18.5 mV) and  $Zn_{0.4}Fe_{2.6}O_4$ -PEG NPs (-2.8 mV) due to the introduction of transmembrane peptides. The improvement of charges promoted the binding of nanoparticles to the cell membrane and uptake by tumor cells.

### Measurement of MRI contrast

$Fe_3O_4$  NPs are known to be as  $T_2$  negative MR contrast agents, which is capable of reducing the MR signal intensity. In this study, we synthesized  $Zn_{0.4}Fe_{2.6}O_4$ -PEG NPs and test the MR performance. The samples were diluted in water with an Fe concentration in a range of 0.1 - 1 mg/mL, and the relaxation time ( $T_1$  or  $T_2$ ) decreased with the increasing concentration of Fe. Depicted in Fig. 6, by plotting relaxation rate as a function of Fe concentration, the  $r_1$  and  $r_2$  of the  $Zn_{0.4}Fe_{2.6}O_4$ -PEG NPs were calculated as

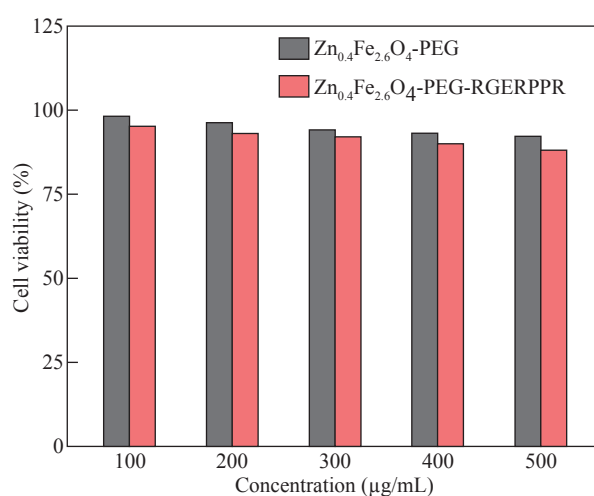
**Table 1** Zeta potential and particle size

Nanoparticles	Zeta potential (mV)	Hydrodynamic size (nm)
Zn <sub>0.4</sub> Fe <sub>2.6</sub> O <sub>4</sub>	-18.5 ± 1.51	52.0 ± 1.22
Zn <sub>0.4</sub> Fe <sub>2.6</sub> O <sub>4</sub> -PEG	-2.8 ± 1.07	108.2 ± 5.48
Zn <sub>0.4</sub> Fe <sub>2.6</sub> O <sub>4</sub> -PEG-RGERPPR	4.7 ± 1.82	110.7 ± 6.90

**Fig. 6** Enhancement in MRI contrast nanoparticles: (a)  $T_1$  relaxivity efficient of Zn<sub>0.4</sub>Fe<sub>2.6</sub>O<sub>4</sub>-PEG NPs; (b)  $T_2$  relaxivity efficient of Zn<sub>0.4</sub>Fe<sub>2.6</sub>O<sub>4</sub>-PEG NPs; and (c)  $T_1$ -weighted MR images.

47.4  $\text{mM}^{-1}\text{s}^{-1}$  and 158.30 respectively. Then,  $r_2/r_1$  ratio was calculated as 3.34, which revealed the superior  $T_1$  contrast performance as the  $r_2/r_1$  ratio was between 3 and 4. Therefore, we tested the MRI performance of the Zn<sub>0.4</sub>Fe<sub>2.6</sub>O<sub>4</sub>-PEG NPs using the MR image with a  $T_1$  mode, and the MR signal intensity of nanoparticles increased with the increasing of Fe concentration, suggesting that the NPs could be used as potential  $T_1$ -weighted positive contrast agents for MR imaging applications.

To further study the biocompatibility of the nanoparticles, we performed a cytotoxicity test. As shown in Fig. 7, after incubating with Zn<sub>0.4</sub>Fe<sub>2.6</sub>O<sub>4</sub>-PEG and Zn<sub>0.4</sub>Fe<sub>2.6</sub>O<sub>4</sub>-PEG-RGERPPR NPs for 24 hours, cell survival rate maintained above 80% and the cytotoxicity was dose-dependent. In addition, compared with Zn<sub>0.4</sub>Fe<sub>2.6</sub>O<sub>4</sub>-PEG NPs, Zn<sub>0.4</sub>Fe<sub>2.6</sub>O<sub>4</sub>-PEG-RGERPPR NPs appeared a slightly decrease of

**Fig. 7** Cell viability of Zn<sub>0.4</sub>Fe<sub>2.6</sub>O<sub>4</sub>-PEG and Zn<sub>0.4</sub>Fe<sub>2.6</sub>O<sub>4</sub>-PEG-RGERPPR NPs at different concentrations by CCK assay.

cell viability, which is due to the reduced membrane translocation activity of RGERPPR. Phospholipids,

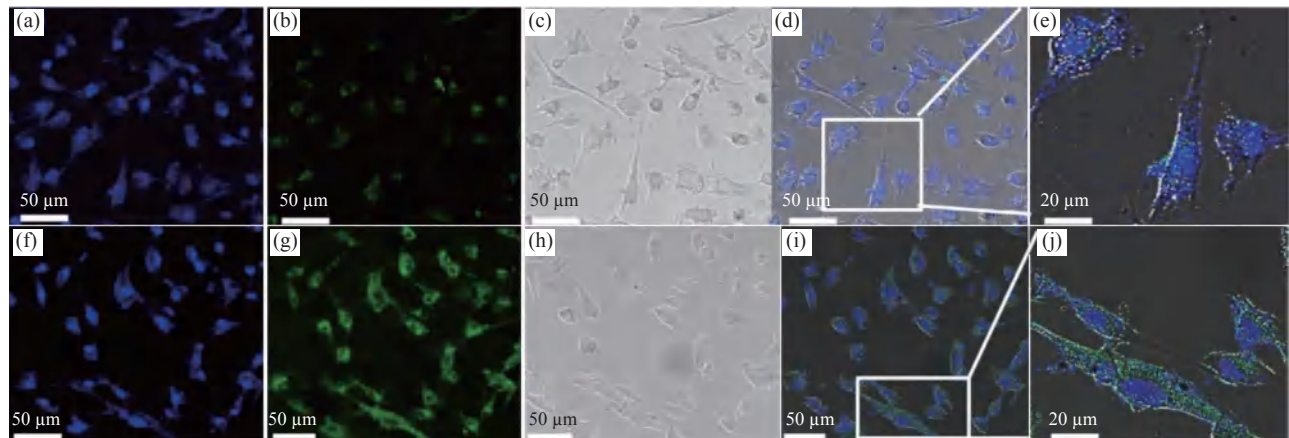


**Fig. 8** Confocal microscopy images of the U87 cells after 8 hours incubation with (a)-(e)  $Zn_{0.4}Fe_{2.6}O_4$ -PEG-FITC and (f)-(j)  $Zn_{0.4}Fe_{2.6}O_4$ -PEG-RGERPPR/FITC NPs. Nuclei were stained with DAPI (blue). Magnetic nanoparticles were detected by reflected laser scanning at 488 nm (green).

as a biosafe material, are relatively harmless to cells. Hydrophilic polyethylene glycol (PEG) and phospholipids (DSPE) used to encapsulate iron oxide nanoparticles, can reduce the biological toxicity of iron oxide. The results showed that the prepared  $Zn_{0.4}Fe_{2.6}O_4$ -PEG and  $Zn_{0.4}Fe_{2.6}O_4$ -PEG-RGERPPR nanoparticles were low-toxic and biocompatible and were suitable for application as biomedical contrast agents.

Cellular uptake of  $Zn_{0.4}Fe_{2.6}O_4$ -PEG was evaluated with U87 cells using laser scanning confocal microscopy. The prepared  $Zn_{0.4}Fe_{2.6}O_4$ -PEG NPs was functionalized with RGERPPR, which is the specific ligand of NRP-1, facilitating the passing of NPs through tumor vessels and stroma. As expected, in Fig. 8,  $Zn_{0.4}Fe_{2.6}O_4$ -PEG-RGERPPR/FITC NPs have been effectively engulfed by U87 cells, and apparent significant higher fluorescent intensity of  $Zn_{0.4}Fe_{2.6}O_4$ -PEG-RGERPPR/FITC NPs in U87 cells has been observed than that of  $Zn_{0.4}Fe_{2.6}O_4$ -PEG-FITC NPs. The confocal imaging indicated that the modification of RGERPPR increased the selectivity and internalization of NPs into the cell through peptide-receptor mediated endocytic pathway.

To explore the *in vivo* performance of the  $Zn_{0.4}Fe_{2.6}O_4$ -PEG-RGERPPR NPs, we studied the ability of nanoparticles to target brain tumors for imaging and diagnostic applications. Fig. 9 shows representative  $T_1$ -weighted images of mice with U87 glioma tumors obtained 1h after injection of saline and nanoparticles at a dose of 10 mg Fe per kg. The MR parameters of images in both groups were identical. RGERPPR NP for 20 min, and only 7.29% of signal

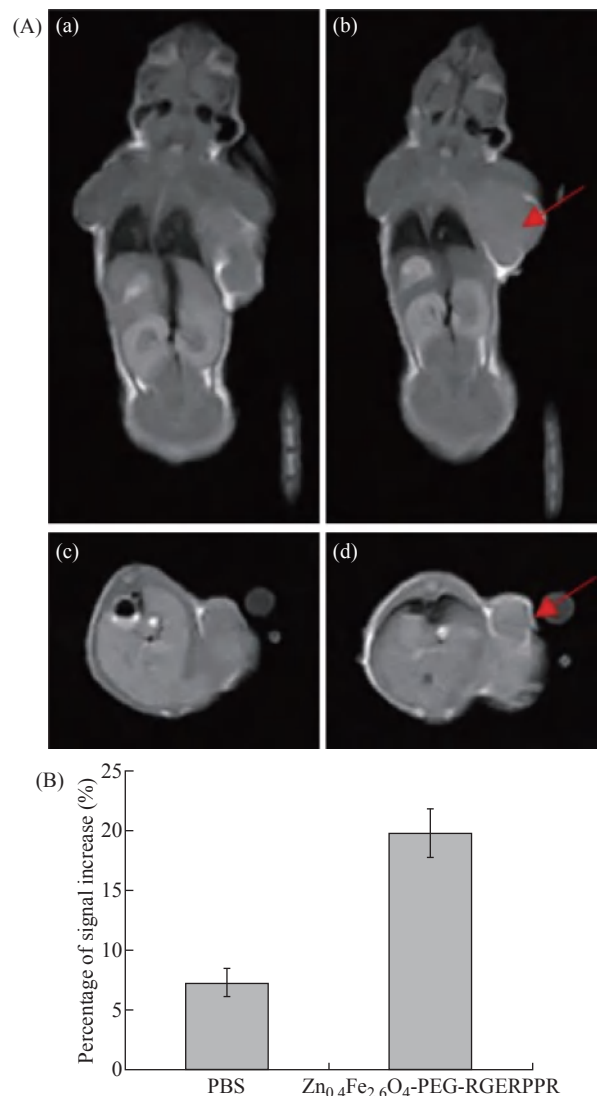


**Fig. 9** (A) U87 tumor-bearing mice  $T_1$ -weighted MR image after injection of (a) and (c) saline and (b) and (d) solution of  $Zn_{0.4}Fe_{2.6}O_4$ -PEG-RGERPPR NPs *in vivo*. (B) Percentage of MRI signal increase after injection of saline and solution of  $Zn_{0.4}Fe_{2.6}O_4$ -PEG-RGERPPR NPs for 20 min.

increase of PBS. This result revealed the higher MR performance of the MRI contrast agents than that of control group.

## Conclusions

In summary, we developed a convenient approach to prepare RGERPPR-modified, liposome-coated iron oxide nanoparticles. The prepared  $Zn_{0.4}Fe_{2.6}O_4$  NPs had highly ordered inverse spinel crystal structure. Surface modification with DSPE-PEG prevented nanoparticles from aggregation and endowing NPs with good water dispersibility, low toxicity and biocompatibility. After surface coating, the particle size was increased from 9 nm to 17 nm which was appreciate for delivery NPs through EPR effect. However, due to relatively small critical pore size, the EPR effect of intracranial tumors is weaker than peripheral tumors, resulting in low delivering efficiency of NPs from blood vessel to cancer tissues. PEGylation also enabled the conjugation of RGERPPR to surface of the NPs, which improved the surface charges of nanoparticles and promoted the internalization of NPs in tumor cells and tissues which induced by vesicle penetrating peptide-receptor mediated NPs delivery. Moreover, MNPs of  $> 5$  nm are typically used as  $T_2$ -weighted MR imaging due to the double-layer of spin-canted structure. Doping of Zinc increases the magnetic saturation strength of iron oxide nanoparticles. The designed nanoparticles demonstrated high efficiency as a  $T_1$ -weighted MRI contrast agent. In vitro laser scanning confocal experiments confirmed the effective cellular uptake ability of the NPs by U87 cells. Meanwhile, the in vivo MRI experiment further proved, increased  $T_1$  signal in tumor regions of mice. These results reveal that  $Zn_{0.4}Fe_{2.6}O_4$ -PEG-RGERPPR NPs exhibit satisfactory MR imaging capacity and could be further exploited as a potential tumor diagnostic agent. In addition, future research on targeted glioma imaging, toxicity and biodistribution are also necessary for the clinical use of this nanoparticle system.

## Acknowledgements

This project was financially supported by the National Key R&D Program of China (2016YFA0201200), National Science Foundation for Young Scientists of China (21807069), Shanghai Outstanding Technology Leader (19XD1431900) and Shanghai Rising-Star Program (19QB1403900)

and Shanghai Biopharmaceutical Support Program (19441910700).

## Conflict of Interests

These authors declare no competing financial interest.

## References

- [1] E. Bleeker, R.J. Molenaar, S. Leenstra. Recent advances in the molecular understanding of glioblastoma. *Journal of neuro-oncology*, 2012, 108(1): 11-27.
- [2] O. Gallego. Nonsurgical treatment of recurrent glioblastoma. *Current Oncology*, 2015, 22(4): e273-281.
- [3] S.B. Ruang, Y. Zhou, X.G. Jiang, H.L. Gao. Rethinking CRITID procedure of brain targeting drug delivery: circulation, blood brain barrier recognition, intracellular transport, diseased cell targeting, internalization, and drug Release. *Advanced Science*, 2021, 8(9): 2004025.
- [4] W.N. Zhang, Z.B. Huang, X.M. Pu, X.C. Chen, G.F. Yin, L. Wang, F. Zhang, F.B. Gao. Fabrication of doxorubicin and chlorotoxin-linked Eu-Gd<sub>2</sub>O<sub>3</sub> nanorods with dual-model imaging and targeted therapy of brain tumor. *Chinese Chemical Letters*. 2020, 31: 285-291.
- [5] S. Giannopoulos, A.P. Kyritsis. Diagnosis and management of multifocal gliomas. *Oncology*, 2010, 79: 306-312.
- [6] S. Mornet, S. Vasseur, F. Grasset, et al. Magnetic nanoparticle design for medical applications. *Progress in Solid State Chemistry*, 2006, 34(2-4): 237-247.
- [7] V.F. Cardoso, A. Francesko, C. Ribeiro, et al. Advances in Magnetic Nanoparticles for Biomedical Applications. *Advanced Healthcare Materials*, 2018, 7: 1700845.
- [8] F. Zhang, X. Huang, L. Zhu, et al. Noninvasive monitoring of orthotopic glioblastoma therapy response using RGD-conjugated iron oxide nanoparticles. *Biomaterials*, 2012, 33(21): 5414-5422.
- [9] Z. Zhou, L. Yang, J. Gao, et al. Structure-Relaxivity Relationships of Magnetic Nanoparticles for Magnetic Resonance Imaging. *Advanced Materials*, 2019, 31(8): e1804567.
- [10] Z. Li, P.W. Yi, Q. Sun, et al. Ultrasmall Water-Soluble and Biocompatible Magnetic Iron Oxide Nanoparticles as Positive and Negative Dual Contrast Agents. *Advanced Functional Materials*, 2012, 22(11): 2387-2393.
- [11] Y. Hu, S. Mignani, J.P. Majoral, et al. Construction of iron oxide nanoparticle-based hybrid platforms for tumor imaging and therapy. *The Royal Society of Chemistry*, 2018, 47(5): 1874-1900.
- [12] J. Mosafer, K. Abnous, M. Tafaghodi, et al. Preparation and characterization of uniform-sized PLGA nanospheres encapsulated with oleic acid-coated magnetic-Fe<sub>3</sub>O<sub>4</sub> nanoparticles for simultaneous diagnostic and therapeutic applications. *Colloids and Surface A: Physicochemical and Engineering Aspects*, 2017, 514: 146-154.
- [13] A.G. Roca, J. F. Marco, M.D. Morales, et al. Effect of nature and particle size on properties of uniform magnetite and maghemite nanoparticles. *Journal of Physical Chemistry C*, 2007, 111(50): 18577-18584.
- [14] N. Lee, T. Hyeon. Designed synthesis of uniformly sized iron oxide nanoparticles for efficient magnetic resonance imaging contrast agents. *The Royal Society of Chemistry*, 2012, 41(7): 2575-2589.
- [15] L.R. Jaidev, D.R. Chellappan, D.V. Bhavsar, et al. Multi-functional nanoparticles as theranostic agents

- for the treatment & imaging of pancreatic cancer. *Acta Biomaterialia*, 2017, 49: 422-433.
- [16] M.A. Abakumov, N.V. Nukolova, M. Sokolsky-Papkov, et al. VEGF-targeted magnetic nanoparticles for MRI visualization of brain tumor. *Nanomedicine*, 2015, 11(4): 825-833.
- [17] M.A. Shevtsov, B.P. Nikolaev, L.Y. Yakovleva, et al. Superparamagnetic iron oxide nanoparticles conjugated with epidermal growth factor (SPION-EGF) for targeting brain tumors. *International Journal of Nanomedicine*, 2014, 9: 273-287.
- [18] P.H. Ai, H. Wang, K. Liu, et al. The relative length of dual-target conjugated on iron oxide nanoparticles plays a role in brain glioma targeting. *Rsc Advances*, 2017, 7(32): 19954-19959.
- [19] C. Sun, C. Fang, Z. Stephen, et al. Tumor-targeted drug delivery and MRI contrast enhancement by chlorotoxin-conjugated iron oxide nanoparticles. *Nanomedicine (Lond)*, 2008, 3(4): 495-505.
- [20] J. Zhang, N. Chen, H. Wang, et al. Dual-targeting superparamagnetic iron oxide nanoprobe with high and low target density for brain glioma imaging. *Journal of Colloid and Interface Science*, 2016, 469: 86-92.
- [21] L. Gao, J. Yu, Y. Liu, et al. Tumor-penetrating Peptide Conjugated and Doxorubicin Loaded T<sub>1</sub>-T<sub>2</sub> Dual Mode MRI Contrast Agents Nanoparticles for Tumor Theranostics. *Theranostics*, 2018, 8(1): 92-108.
- [22] X. Zhao, T. Shang, X. Zhang, et al. Passage of Magnetic Tat-Conjugated Fe<sub>3</sub>O<sub>4</sub>@SiO<sub>2</sub> Nanoparticles Across In Vitro Blood-Brain Barrier. *Nanoscale Research Letters*, 2016, 11(1): 451.
- [23] V.S. Perera, G. Covarrubias, M. Lorkowski, et al. One-pot synthesis of nanochain particles for targeting brain tumors. *Nanoscale*, 2017, 9(27): 9659-9667.
- [24] W. Jiang, H. Xie, D. Ghoorah, et al. Conjugation of functionalized SPIONs with transferrin for targeting and imaging brain glial tumors in rat model. *PLoS One*, 2012, 7(5): e37376.
- [25] Y. Luo, J. Yang, Y. Yan, et al. RGD-functionalized ultrasmall iron oxide nanoparticles for targeted T<sub>1</sub>-weighted MR imaging of gliomas. *Nanoscale*, 2015, 7(34): 14538-14546.
- [26] T. Schlorf, M. Meincke, E. Kossel, et al. Biological properties of iron oxide nanoparticles for cellular and molecular magnetic resonance imaging. *International Journal Molecular Sciences*, 2010, 12(1): 12-23.
- [27] M.K. Yu, J. Park, S. Jon. Targeting strategies for multifunctional nanoparticles in cancer imaging and therapy. *Theranostics*, 2012, 2(1): 3-44.
- [28] M. Ying, Q. Shen, Y. Liu, et al. Stabilized Heptapeptide A7R for Enhanced Multifunctional Liposome-Based Tumor-Targeted Drug Delivery. *ACS Applied Materials & Interfaces*, 2016, 8(21): 13232-13241.
- [29] T. Teesalu, K.N. Sugahara, V.R. Kotamraju, et al. C-end rule peptides mediate neuropilin-1-dependent cell, vascular, and tissue penetration. *Proceedings of the National Academy of Sciences of the United States of America*, 2009, 106(38): 16157-16162.
- [30] J. Rieger, W. Wick, M. Weller. Human malignant glioma cells express semaphorins and their receptors, neuropilins and plexins. *Glia*, 2003, 42(4): 379-389.
- [31] L. Simon-Gracia, H. Hunt, P. Scodeller, et al. iRGD peptide conjugation potentiates intraperitoneal tumor delivery of paclitaxel with polymersomes. *Biomaterials*, 2016, 104: 247-57.
- [32] Y. Yang, Z. Yan, D. Wei, et al. Tumor-penetrating peptide functionalization enhances the anti-glioblastoma effect of doxorubicin liposomes. *Nanotechnology*, 2013, 24(40): 405101.
- [33] W.J. Mulder, G.J. Strijkers, A.W. Griffioen, et al. A liposomal system for contrast-enhanced magnetic resonance imaging of molecular targets. *Bioconjugate Chemistry*, 2004, 15(4): 799-806.

**Copyright**© Weijia Chen, Yingtian Xu, Dicheng Yang, Ping Wang, Yan Xu, Jun Zhu, and Daxiang Cui. This is an open-access article distributed under the terms of the Creative Commons Attribution License, which permits unrestricted use, distribution, and reproduction in any medium, provided the original author and source are credited.